9th International Conference on Numerical Ship Hydrodynamics
Ann Arbor, Michigan, 5-8 August 2007

Optimal Shape for Forces and Moments on a Multi-Element Hydrofoil

Yu-Tai Lee[1], Vineet Ahuja[2], Ashvin Hosangadi[2] and Michael P. Ebert[1]
([1]Naval Surface Warfare Center, Carderock Division, [2]CRAFT Tech, Inc., U.S.A.)

ABSTRACT

A movable flap with a symmetric NACA foil serves as a common control surface for underwater marine vehicles. To augment the functionality of the control surface, a Tab-Assisted Control (TAC) surface was experimentally tested to address its benefits to various different requirements of the control surface. The advantage of the TAC surface could be further enhanced with Shape Memory Alloy (SMA) actuators to control the rear portion of the control surface to form a flexible tab (or FlexTAC) surface. Although the measured FlexTAC data demonstrated similar augmentation in enhancing an airfoil's functionality, they also show subtle differences in data obtained from the TAC and FlexTAC measurements.

High fidelity hybrid unstructured Reynolds Averaged Navier Stokes (RANS) calculation results are used to define the flow fields associated with the multi-element FlexTAC foil with a stabilizer, a flap and a flexible tab. The prediction results are compared with the measured data obtained from both the TAC and the FlexTAC experiments. The comparison also leads to the resolution of the differences that existed between the two data sets. In addition the RANS solutions are validated for predicting the forces and moments acting on the hydrofoil with adequate accuracy for use with an optimization scheme.

For a horizontal control surface to effectively provide upward and downward motions, it is necessary to maintain a symmetric foil shape. In order to achieve maximum benefit out of a horizontal TAC/FlexTAC surface, a shape modification of the stabilizer (fixed portion of the hydrofoil) and the flap is desirable to account for the requirements at the most severe scenario. This paper focuses on the conditions when the movable flap surface becomes jammed. Since the present investigation deals with a FlexTAC configuration with a flexible tab, the shape modification focuses only on the stabilizer and the non-flexible portions of the flap.

The shape optimization calculations coupling with the RANS predictions use an evolutionary algorithm, which consists of a genetic algorithm based design optimization procedure. This procedure searches the complex design landscape in an efficient and parallel manner. Furthermore, it can easily handle complexities in constraints and objectives and is disinclined to get trapped in local extreme regions. The utilization of the hybrid unstructured methodology provides flexibility in incorporating large changes in shape. The mesh regeneration is carried out in an automated manner through a scripting process within the grid generator. The optimization calculation is performed simultaneously on both the stabilizer and the flap. Shape changes to the trailing edge of the stabilizer strongly influence the secondary flow patterns that set up in the gap region between the stabilizer and the flap. These are found to have a profound influence on force and moment characteristics. Experimental and numerical evaluations of a shape obtained from a study of optimization results on the Pareto front for the current optimization landscape, further validating the optimization objectives.

INTRODUCTION

The Tab Assisted Control (TAC) foil used for underwater control surfaces, shown in Fig. 1a, was tested in the 24-inch water tunnel at the David Taylor Model Basin (DTMB) in 1998. Results of Nguyen et al. (1999) indicate that the addition of a tab to regular control surfaces can enhance their capabilities through significant modification of lift and torque on the control surfaces.

The benefits of the TAC concept can be further augmented by using Shape Memory Alloy (SMA) actuators (Carpenter and Nguyen, 1999) shown in Fig. 2 and shape optimization (Cao and Blom, 1996) for the complete control surfaces. Employing SMA actuators enables the use of electric power to manipulate the control surfaces, and eliminates the need for hydraulic systems and the gap between the flap and the tab. These advantages led to the development of the Flexible Tab Assisted Control

(FlexTAC) surfaces for marine applications. The optimization effort aims to numerically achieve optimized designs for future FlexTAC foil applications.

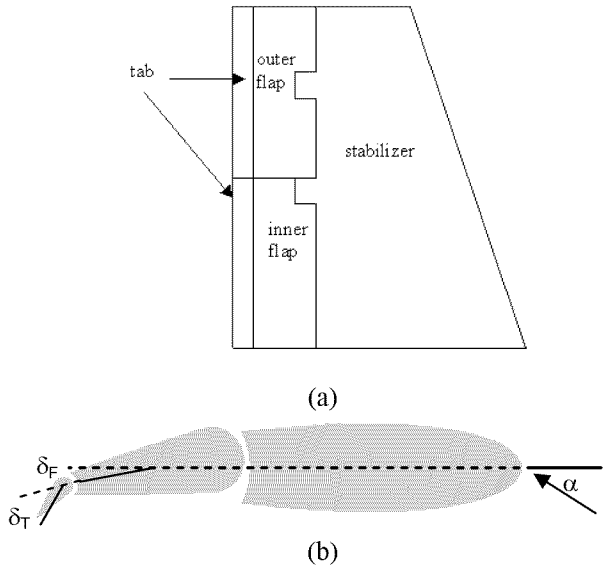

Figure 1: Schematics of TAC foil tested in the 24" water tunnel (a) overall foil (b) a cross section with defined angles

Figure 2: Foil instrumented and actuated with SMA wires

The TAC foil shown in Fig. 1 contains (1) a pedestal to minimize the water-tunnel bottom-wall boundary-layer effect on the measured forces and moments; and (2) gudgeons to connect the stabilizer, the flap and the tab, and to control their relative motions. These gudgeons also affect the gap flow fields. The FlexTAC foil experiment (Gowing et al., 2004) conducted during 2002 in the DTMB's 36-inch water tunnel did not have the pedestal and gudgeons as shown in Fig. 3. The length of the flexible tab, accounting for 20 % of the flap foil chord, was developed based on an early optimization calculation (Lee et al., 2003). Also the stabilizer for the FlexTAC experiment was installed with a turbulent-flow stimulator near the foil's leading edge. Although the two experiments deal with similar foil shapes, which have similar augmentation in enhancing the forces, they show subtle difference in the torques produced.

Sung et al. (1999 and 2000) used a CFD tool to predict forces and moments on the TAC foil. The agreement of their CFD results with the measured data is good, but the comparisons are restricted to the linear portion of the data. Although three relative angular settings between the stabilizer, flap and tab were studied experimentally, the numerical investigations (Sung et al., 2000) were limited to only one angular position for each comparison. In addition, the effects of the gaps between the stabilizer and the flap and between the flap and the tab were neglected in that study. In the present paper two high fidelity unstructured RANS codes (Hosangadi et al., 1996 and Hyams et al., 2002) are used to predict flow fields associated with both TAC and FlexTAC foils. The predictions are compared with the measured data obtained from both experiments. The comparisons not only lead to the resolution of the differences existed between the two data sets, but also provide the validation that demonstrates the predicted forces and moments acting on the foil are predicted with adequate accuracy for use with an optimization calculation.

Early work (Lee et al., 2003) of optimization calculations for the multi-element foil provided guidelines in choosing the length for the flexible tab in constructing the FlexTAC foil shape. The resulting foil shapes were, however, not realistic due to the deficiency in locating the global maximum or minimum with a gradient scheme for the search process. In the present paper, an evolutionary algorithm is adapted with the RANS coupling. This evolutionary scheme uses a genetic algorithm based design procedure. It has the advantage of easily handling complex constraints and objectives and avoiding local extremes. The utilization of the hybrid unstructured methodology provides flexibility in incorporating large changes in shape. The mesh regeneration is carried out in an automated manner through a scripting process within the grid generator. The optimization calculation is performed simultaneously on both the stabilizer and the flap. The resultant shapes selected from the Pareto front investigation of the optimization landscape are compared. An OptimTAC was chosen for further CFD and experimental validations.

UNSTRUCTURED CFD SCHEMES AND GRIDS

Two computational approaches were used to investigate predictive capabilities for the FlexTAC and the TAC airfoils. Both approaches perform RANS calculations on a computational domain extending 2 chord lengths upstream and 4.5 chords downstream of the airfoil, 3 chord lengths in the transverse direction, and 2 chord lengths in the spanwise direction.

The first RANS approach uses the unstructured U2NCLE code (Hyams et al., 2002). U2NCLE solves the incompressible Navier Stokes equations with artificial compressibility. The flow solver uses a node-centered, finite volume, implicit time-marching

scheme. The flow variables are stored at the vertices. A one-to-one mapping is used to convert edge information to the faces of the control volumes. U2NCLE is programmed for parallel processing, using MPI for interprocessor communication and a coarse-grained domain decomposition for concurrent solution within subdomains assigned to multiple processors. A two-equation q-ω turbulence model (Coakley and Hsieh, 1985) is used for the present work.

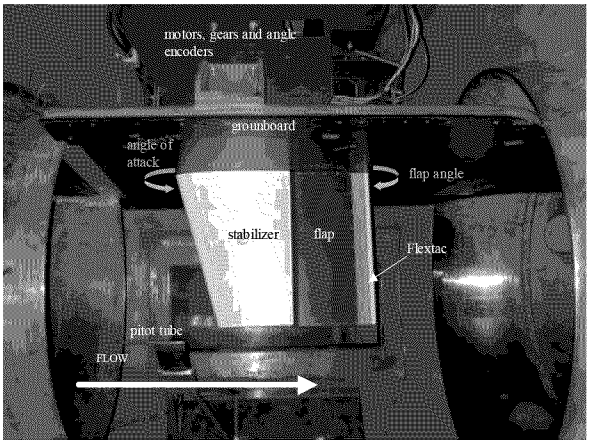

Figure 3: FlexTAC foil in the 36" water tunnel

The grids used for the U2NCLE calculations are multi-element unstructured grids generated using an advancing normal methodology for the boundary layer elements and an advancing front/local reconnection (AFLR) methodology (Marcum and Weatherill, 1995) for the isotropic tetrahedral elements. Surface grid generation and geometry preparation were accomplished using SolidMesh (Gaither et al., 2000). Special attention was paid to the grid spacing in the gaps between the stabilizer, flap and tab to avoid poor grid quality. The gudgeons are not modeled in these calculations, resulting in airfoil elements that are completely disconnected from each other. A symmetry boundary condition is applied on the plane formed by the root section of the airfoil and a far-field boundary condition is employed at a sufficient distance away from the wing to avoid any influence on the solution. The grids on the TAC symmetry plane and the FlexTAC gap are shown in Fig. 4. Near-wall y^+ is maintained close to unity for the turbulence model used. The total number of cells for each grid is around 3.5 million.

The second RANS approach uses the unstructured CRUNCH code (Hosangadi et al., 1996 and Ahuja et al., 2001). The CRUNCH code solves incompressible Navier Stokes equations using a finite-volume Roe/TVD flux construction based on the cell-vertex formulation. The numerical integration uses explicit four-stage Runge-Kutta, implicit GMRES, and Gauss-Seidel schemes. The code works for multi-element grids including tetrahedral, hexahedral, prismatic and pyramid cells. CRUNCH is also programmed for parallel processing, using MPI and an automated load balancing domain decomposition. A dynamic grid capability (Cavallo et al., 1997), which is essential for coupled optimization calculations, using a node movement solver is available for automated embedding and sliding interfaces. A two-equation k-ε turbulence model (So et al., 1997) with a wall-function approach is used for the current calculations.

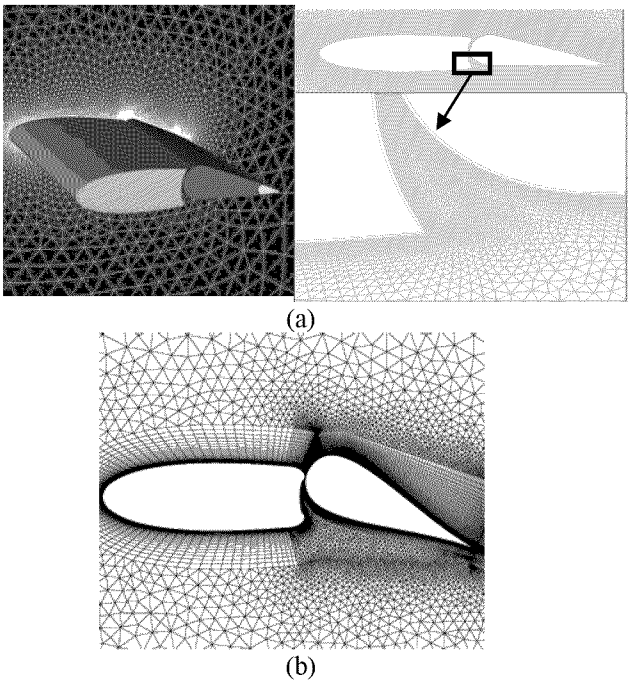

Figure 4: Grids for TAC and FlexTAC foils (a) unstructured; (b) hybrid

The grids used for the CRUNCH calculations were generated using GRIDGEN. They consist of hexahedral, tetrahedral and prismatic hybrid elements with approximately 2.5 million cells. The pedestal and the gudgeons are not modeled for the TAC foil calculations. The outer domains are treated with far-field boundary conditions. The foil root surface is treated as an inviscid wall due to the use of the pedestal for the TAC experiment.

FLOW CONDITIONS AND CFD VALIDATION STRATEGY

The CFD simulations presented in this paper include both TAC and FlexTAC foils.

For the TAC foil, the tip chord is 0.213 m (8.40 inches), the base chord 0.271 m (10.66 inches), and the span 0.214 m (8.44 inches). Both the flap and tab gaps are 0.159 cm (1/16 inch) with the flap gap widened at both ends. The computational grid is non-

dimensionalized by the mean chord length at mid span, which is 0.242 m (9.526 inches). The Reynolds number based on the mean chord and a flow speed of 3.392 m/s (11.13 ft/s) is 9.7 x 10^5. Hinge points for torque calculations are located at x = 0.3085 for the stabilizer, x = 0.8011 for the flap, and x = 1.0186 for the tab in non-dimensional units. The origin of the coordinate is at the leading edge of the base. Note that the experimentally installed pedestal and the gudgeons are not modeled, as mentioned in the previous sections. The deflection angles, shown in Fig. 1b, for the stabilizer (α), the flap (δ_F) and the tab (δ_T) are measured with respect to the incoming flow, the stabilizer and the flap, respectively. The measured ranges of α, δ_F, and δ_T are from –15 to 15 degrees, from –27 to 27 degrees, and from –60 to 60 degrees, respectively.

For the FlexTAC foil, the dimensions are normalized by the mean chord of 0.503 m (19.791 inches). The pre-test calculations were performed at a nominal speed of 3.048 m/s (10 ft/s) and a Reynolds number of 1.833 x 10^6. The test was later performed at a lower speed of 2.59 m/s (8.5 ft/s) due to limitations of the SMA wires.

The current approach of using an unstructured grid methodology aims to achieve gridding flexibility in the gap region and also to enable grid movement for the foil shape modification during automated numerical optimization. Two flow conditions were investigated to validate the abilities of U2NCLE and CRUNCH to predict general flow features and the gap effect. These two cases are:

Case A: α = 0 deg., δ_T = 0 deg., δ_F varying between –27 and 27 degrees

Case B: α = 6 deg., δ_T = 0 deg., δ_F varying between –27 and 27 degrees

All cases are within the normal range of the control-surface operation. Case A is the baseline case with relative motion only between the stabilizer and the flap. Case B is similar to Case A, but with an angle of attack specified for the stabilizer. Since there is no exact correspondence between the FlexTAC and TAC foils in δ_F, it is set to be zero. Case A is used to validate the predictability and grid density effects between the two RANS codes. Only results of Case B are shown here. Results of other cases are given in Lee et al. (2003).

CFD COMPUTATIONAL RESULTS

The 24-inch water-tunnel measurements (Nguyen et al., 1999) for the TAC foil include overall lift and drag on the foil and torques acting on the stabilizer, the flap with the tab, and the tab, respectively. These measured quantities are compared to the predictions in a non-dimensional form based on the mean chord (c_m) and the water tunnel speed V_∞. They include lift and drag coefficients (normalized by ½ ρ V_∞^2 c_m^2) and stabilizer, flap and tab torque coefficients (normalized by ½ ρ V_∞^2 c_m^3).

The 36-inch water tunnel tests (Gowing et al., 2004) for the FlexTAC foil measured similar quantities as for the TAC foil. Since the profile shapes of the flexible portion of the FlexTAC foil were not known a priori, the pre-tested predictions were done with the assumption that the airfoil was rigid.

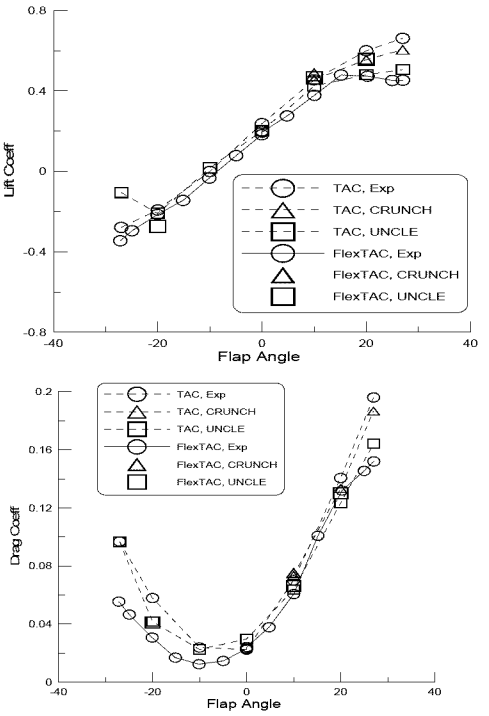

Figure 5: Force comparisons for TAC and FlexTAC airfoils

The comparisons are plotted in Figs. 5 and 6. Note that blue symbols are used for the TAC airfoil data and red symbols for the FlexTAC airfoil data. The measured FlexTAC lift and drag are lower than the measured TAC values, particularly for flap angles less than 0 deg. and greater than 18 deg. The predicted FlexTAC lift and drag values are generally higher than the measured values. This suggests that the measured FlexTAC forces may have been over-corrected for the water-tunnel blockage effect (Gowing et al., 2004). Although the blockage correction is perhaps too large, the measured FlexTAC drag at $\alpha = \delta_F = \delta_T = 0$ is 0.0162, which is 35 % higher than the measured TAC drag of 0.01202. This is believed to be from the contribution of the turbulent stimulator installed in the FlexTAC experiments. Figure 6 shows the stabilizer and flap torque comparisons. There are clearly different trends between the FlexTAC and the TAC airfoils. The CFD calculations predict the trend of the

FlexTAC experiments correctly. The effects of the gap flow and the gudgeons on the torque calculations are obvious from the differences between the two measured data sets with and without the gudgeons. The differences were further confirmed by the agreement between the FlexTAC measurements and the CFD predictions, both without gudgeons.

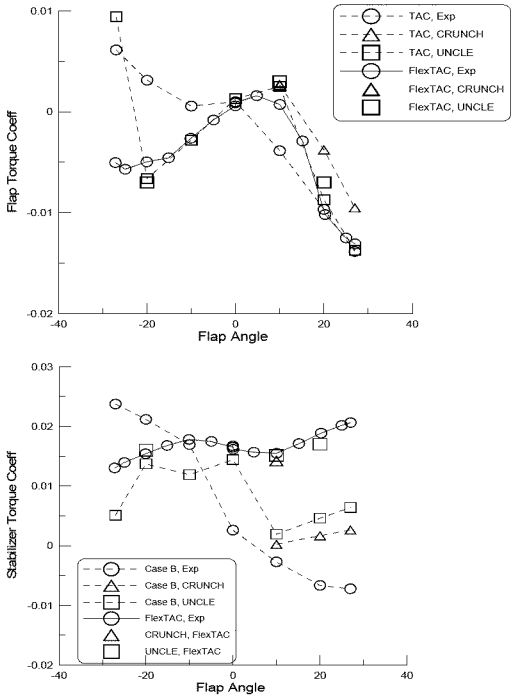

Figure 6: Moment comparisons for TAC and FlexTAC foils

Figure 7 shows pressure distributions for $\alpha = 0$ at the positive flap angles. They clearly indicate that flow separates on the suction side for flap angles between 10 and 20 degrees. The vortex structures shed from the pressure-side trailing corner of the stabilizer (refer to Fig. 12) fill the gap void for larger flap angles and move the pressure-side peak on the flap pressure distribution further downstream due to an increase in size of the gap region. They also provide feedback to the trailing corner area of the stabilizer. All these phenomena indicate that the front gap between the stabilizer and the flap has a dramatic effect on the local flow field, particularly near the leading edge of the flap (which has the pressure peak on the pressure side) and the trailing corner of the stabilizer. In comparisons for cases of non-zero δ_T (Lee et al., 2002), the rear gap effect, however, is not as pronounced as the front gap effect.

A flow visualization at $\alpha = 6$ deg., $\delta_F = 10$ deg., and $\delta_T = 0$ deg. was also made for the FlexTAC foil to further validate the CFD predictions in the foil tip region. Figure 8 shows pressure-side paint traces compared to predicted particle traces on the pressure-side surface. The two paint trace photos zoom in to the flap portion in order to see the detailed streamline pattern. The installation of the sand-grain turbulent stimulator is clearly shown on the stabilizer. The tip flow from the pressure side to the suction side is also visible in both traces. The stagnation line at the leading edge of the flap is shown in the prediction, but was difficult to capture in the experiment due to the high viscosity of the paint.

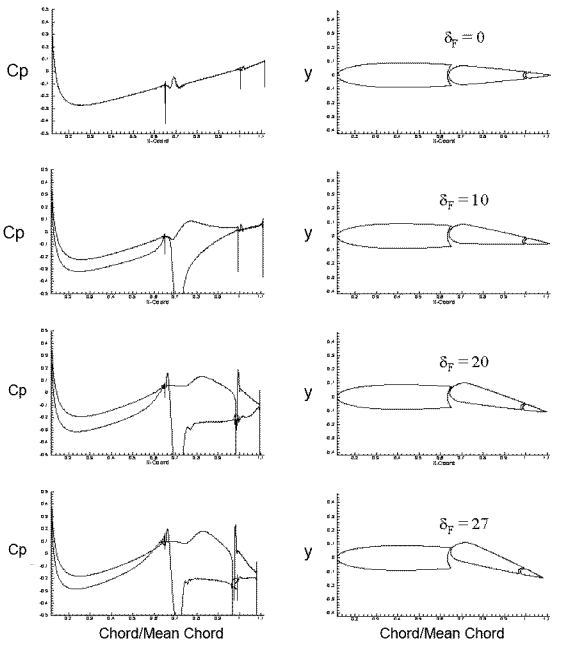

Figure 7: Loading distributions (pressure coefficient versus fraction of chord) on stabilizer and flap for various flap angles

The comparisons shown above illustrate that both CFD predictions deviate from the measured data for flap angles greater than 20 deg., but CRUNCH predicts more accurate forces while U2NCLE predicts more accurate moments.

METHOD OF OPTIMIZATION

Genetic algorithms are adapted for the current multi-element foil shape optimization. The key ideas of how design unfolds in nature in an efficient, parallel and multi-modular manner satisfying a complex network of constraints, variables and objectives are embodied in the workings of genetic algorithms. Formal presentation of the ideology is based on seminal work of Holland (1975) that structures based on chromosome-like strings of binary switches could trigger more favorable characteristics in systems if the chromosomes were permitted to interact with other similar structures based on some measure of fitness,

thereby, reproduce and mutate leading to offspring systems that were better adapted to the environment.

The design procedure is started by taking a stochastic representation of possible designs from the design space and carrying out fitness evaluations utilizing RANS analyses concurrently on all the designs. Designs evolve with the use of the selection, crossover and mutation operators on the design space in a manner analogous to evolution in nature.

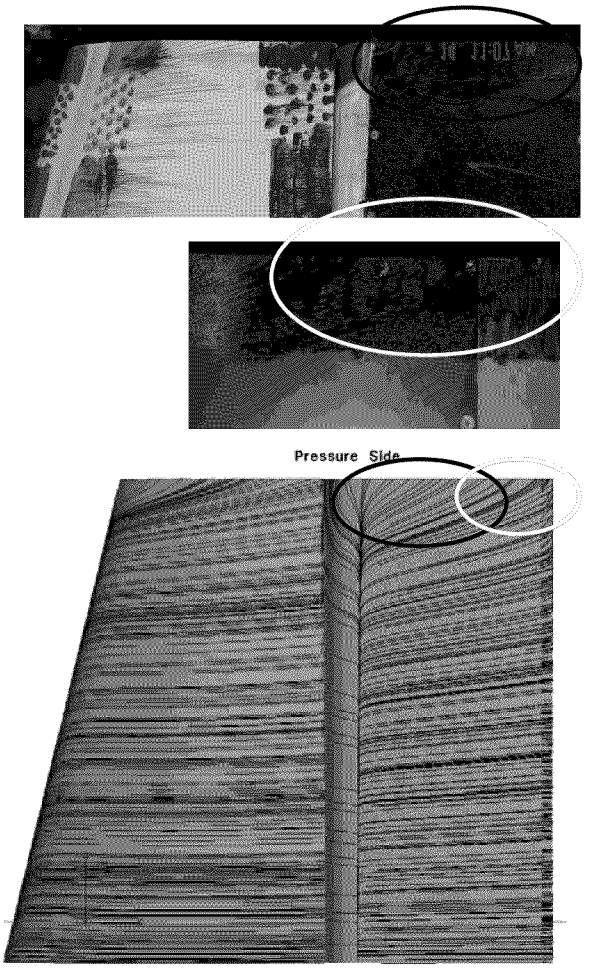

Figure 8: Comparison of water-tunnel paint traces with predicted surface particle traces

The CRUNCH code is used for fitness evaluations. Since genetic algorithms effectively search the entire design space, the geometry can undergo radical changes, thereby requiring a new grid to be generated. For each design, a new grid is generated through a semi-automated grid generation procedure utilizing the scripting language in GRIDGEN. A scripting language TCL/TK interfaces with the grid generator that permits various facets of the grid generation topology such as grid points, shapes of curves, control points, clustering to be specified as variables. Shape deformation in the form of Bezier control points is passed from the genetic algorithm to the TCL/TK script that invokes the grid generation process. The success of the scripted grid generation process is dependent on the use of the same topology for mesh generation of all the designs involved. Multi-element hybrid meshes used by the CRUNCH code and its dynamic gridding capability (Cavallo et al., 1997)) provide significant flexibility to achieve this without any conflicts or distorted grids. Meshes for the new designs are verified for skewness and positive volumes. The topology is modified to accommodate any cellular distortions automatically.

In our studies, the trailing edge of the stabilizer is defined as a cubic Bezier curve with the coordinates of the control points being defined as design variables. Furthermore, the entire curve representing the upper section of the flap is defined as a combination of piecewise Bezier cubic curves. The control points of the Bezier representation also serve as design variables. In all, a combination of seven design variables was considered. Two design variables defined the control points of the Bezier curve representing the trailing edge of the stabilizer and the remaining five variables represented the control points of the piecewise Bezier cubic curves defining the entire surface of the symmetric flap. The curves were defined in such a manner that special emphasis was put on the leading edge (nose thickness) and the trailing edge of the flap and the stabilizer. Since the flap geometry is constrained to be symmetric the lower section is extracted as a mirror image of the redefined upper section. Since the aim of the control surface is torque reduction, the objective function is defined to be the torque at the largest flap angle of operation (25 degrees). In order to eliminate designs that show reduction in torque with substantial reduction in lift, penalty functions were applied to all designs where the flap lift was less than 20% of the baseline flap lift. The other important constraint taken into consideration was preserving the direction of the torque. Penalty functions were also utilized to discard any designs that changed the direction of the torque from the baseline design. Simulations pertaining to fitness evaluations were performed with a Reynolds Number of 1.8 million and a characteristic velocity of 3.05 m/s. Flow was assumed to be incident on the multi-element airfoil at 6 degrees and the flap angle was set at 25 degrees.

OPTIMIZATION CALCULATIONS AND RESULTS

A population size of 16 designs was considered for the genetic algorithm based optimization procedure. All design variables were binary coded. The resulting

fitness function based on the torque of the flap asymptotes after the 5th generation to torque values that are more than three orders of magnitude smaller than the baseline flap section.

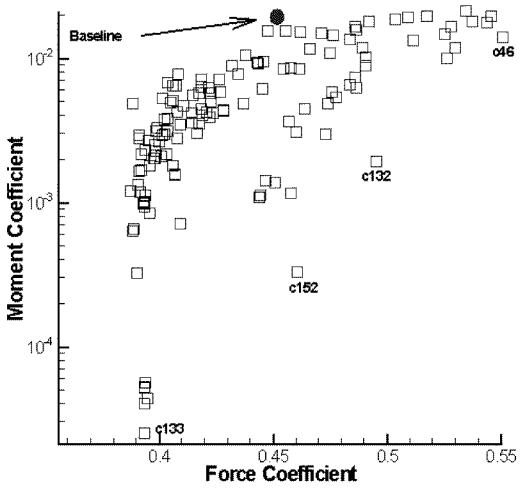

Figure 9: Design landscape showing relative performance of flap characteristics for all shapes utilized by the genetic algorithm

Although the optimized design reduced the flap torque by almost three orders of magnitude for the 16 generation designs, the resulting flap lift coefficient on the optimized design reduced from 0.45 to 0.39. From a practical standpoint, a more attractive design point would be one that provided a reduction in flap torque with an increase in the flap (or flap and stabilizer combined) lift characteristics. Furthermore, sustaining such favourable characteristics over the entire operational range would yield a design far superior to the baseline design. A survey of the entire design landscape shown in Fig. 9 indicates a front of potential design candidates that simultaneously show better force and moment characteristics. The first of these potential candidates labelled C132 has a torque coefficient that is an order of magnitude lower than the baseline design and a 10% increase in flap force coefficient. The second potential candidate labelled C46 in Fig. 9 shows a 30% reduction in flap torque while providing more than 20% increase in flap lift. Such a design is useful because it provides an avenue for operating at a lower flap angle to achieve the same lift generated by a 25 degree flap angle in the case of the baseline design. It should be noted that the design landscape shown in Fig. 9 represents the database of simulations performed for all the design points during the genetic algorithm based optimization for minimizing the flap torque.

Parametric simulations were performed on the cases identified above (C132 and C46) at three different flap angles (25, 20 and 10 degrees) and the performance was compared against the baseline design (See Fig. 10). Consistent with the findings for the 25 degree cases, the flap lift was found to be either vastly improved or close to the baseline flap design lift. In particular, the design for the C46 case consistently proved to show improved flap lift coefficients over the baseline design (improvements ranged from 15% to 22%) throughout the operating range. The multi-element airfoil design pertaining to C132 showed improvement in flap lift by about 10% over the baseline design at the higher angle, however it deteriorated at the lower flap angles. This deterioration is primarily due to the smaller nose region of the flap, which changes the flow blockage characteristics on the suction side leading to a smaller pressure drop. Although, the flap in the C46 has a similar nose, the taper in that design from the mid-chord to the trailing edge dramatically increases the lift at lower angles in that case. The increase in lift at the higher flap angles is accentuated for both the C132 and C46 stabilizer and flap designs. This increase is primarily due to the improvement in the suction side performance on the stabilizer at the higher flap angles (See Figs. 13 and 14). Similarly, the flap torque for the three designs as a function of flap angle is shown in Fig. 11. The flap torque dramatically increases for the baseline design at the higher flap angles of operation. By contrast, the C46 design increases only slightly with flap angle, although it shows an increased flap torque at a flap angle of 10 degrees over the baseline design. Interestingly, the C132 design shows a flat torque profile with variation in flap angle. Moreover, the flap torque is orders of magnitude smaller than the torque for both the other designs. This is a highly desirable feature since it indicates that the power required by the motor to change the operating angle is substantially less during the entire operating regime.

A detailed discussion of the C132 and C46 designs and associated flowfields is provided here. Figure 12a-c depicts a back-to-back comparison of the axial velocity distributions in the flowfields related to the baseline, C132 and C46 designs at a flap angle of 25 degrees. The three designs show significant variation in geometry of the stabilizer and the flap. The baseline design has a sharp trailing edge on the stabilizer and the stabilizer and flap together represent a symmetric NACA airfoil shape. The C132 design comprises of a stabilizer with a well-rounded trailing edge and a flap with a relatively smaller nose region. The C132 flap design, however, is more bulbous (increased thickness) than the baseline design for most of its chord. The C46 design is representative of a stabilizer that is slightly rounded and a flap that is, like the C132 design, smaller in the nose region. However, unlike the C132 design, the C46 flap tapers towards the trailing edge of the flap,

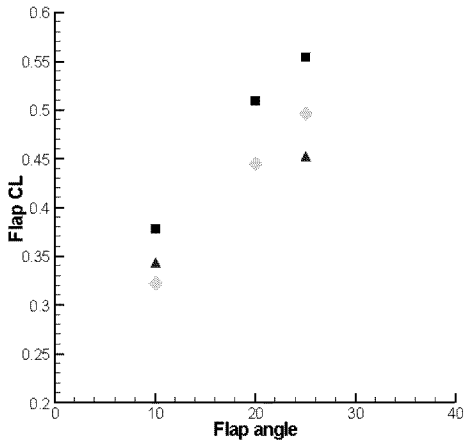

Figure 10: Flap lift coefficient comparison for baseline in red, C132 in green and C46 in blue

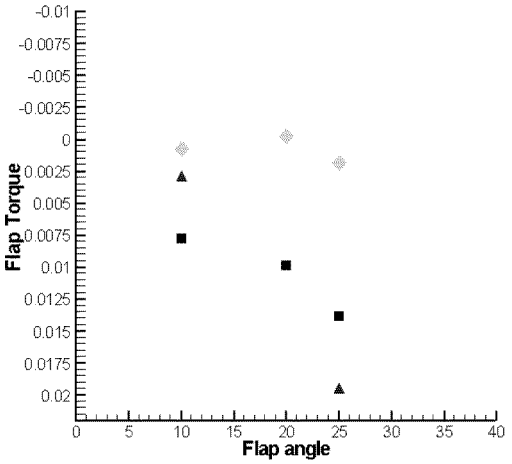

Figure 11: Flap torque coefficient comparison for baseline in red, C132 in green and C46 in blue

thereby showing a reduction in thickness compared to the baseline flap design. A comparison of the axial velocity distributions of the three designs reveals a smooth transition between the flap and stabilizer on the suction side for the C132 and C46 designs. This is primarily due to a combination of the rounding of the stabilizer trailing edge and the smaller nose of the flap. As a consequence of the smooth transition through the gap region on the suction side, the pressure distribution on both the flap and the stabilizer are altered considerably. For example, the pressure on the suction side of the stabilizer is lowered throughout the length of the stabilizer for both the C132 and C46 designs (See Figs. 13 and 14) and the strong adverse pressure gradient close to the suction side trailing edge seen in the baseline design is to a large extent alleviated. This leads to the enhanced combined (stabilizer+flap) lift for the two designs. Furthermore, the velocity distributions in Fig. 12 also indicate that both the C132 and C46 designs have a smaller wake region behind their respective flaps. On the pressure side of the flap the velocity recirculation in the gap region is much smaller for the C132 and C46 designs as the flow comes off smoothly over the rounded stabilizer trailing edges. This causes the high pressure stagnation region to shift forward in the C132 and C46 cases and is primarily responsible for the improved torque characteristics of the two designs. The surface pressure distributions on the stabilizer and flap for the C132 and C46 design cases are plotted against the baseline design in Figs. 13 and 14. The trends in these plots corroborate the findings discussed above: (a) better suction side performance on both the stabilizer and the flap (b) shift in the peak pressure location resulting in a reduction in torque (c) change in gap pressure distribution and (d) significant increase in lift provided by the tapering close to the trailing edge in the C46 design case.

VALIDATION OF OPTIMIZED SHAPE

The current objective of the optimization calculations is to design the multi-element foil with a minimum torque under the large flap angle of 25 degrees. We therefore adopt C132, also named as the OptimTAC, for further numerical and experimental validation even though the computed lift force obtained from the RANS calculations for the 2-D cross section foil is slightly smaller than the original foil at smaller flap angles (Fig. 10).

The aforementioned optimization calculations were performed for the 2-D cross sections to reduce the computational time required by the 3-D RANS calculations. In order to validate the OptimTAC foil's performance, the original FlexTAC gridding setup was replaced with the OptimTAC foil. The force and moment curves of the OptimTAC foil are compared with the baseline FlexTAC foil in Figs. 15 and 16 for $\alpha = 6$ degrees. The predicted FlexTAC foil lift in Fig. 15a is higher than the measurements. The OptimTAC foil lift is slightly higher than the FlexTAC at higher flap angles, but it is about 20% lower at 10^{o} flap angle. The drag in Fig. 15b for the OptimTAC is consistently lower than the FlexTAC for all flap angles. The stabilizer and flap torques in Fig. 16 shows the OptimTAC foil again has lower values at larger flap angles than the FlexTAC foil. For smaller flap angles, the OptimTAC foil encounters larger torque. The general trends for force and moment are consistent with the results obtained through 2-D calculations. However, the nearly constant torque curve for the 2-D OptimTAC flap torque (Fig. 11) has been modified with a monotonically decreasing curve in the 3-D results. Also shown in Fig. 16b are the

measured flap torques (designated as Dyn Exp) on both FlexTAC and OptimTAC foils when both foils were attached to an underwater vehicle and the flap was deflected at 25 degrees. This last measured dynamic data are smaller than the static water-tunnel data. The comparison between the two foil data in the Dyn Exp again confirms the benefit of the OptimTAC design at the high flap angle.

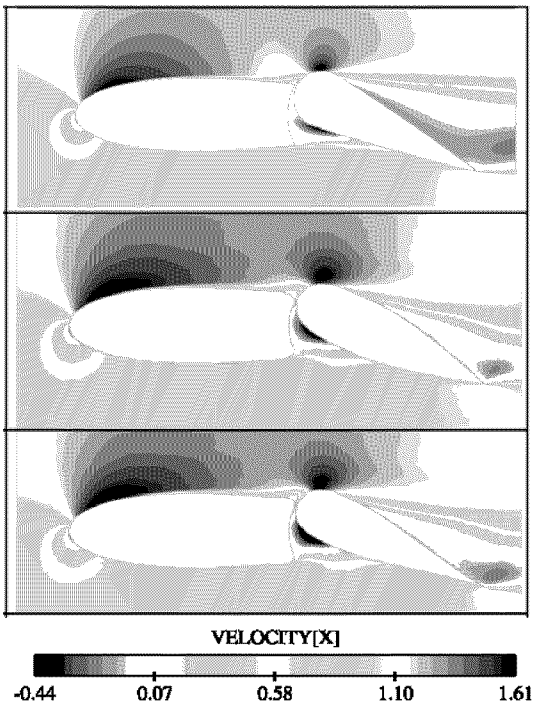

Figure 12: Comparison of the axial velocity distribution between baseline (top), C132 (middle) and C46 (bottom) designs

CONCLUSIONS

The TAC and FlexTAC airfoils, based on symmetric NACA sections, are conceptual designs for future marine vehicle control surfaces. In addition to the relative motion between the flap and the stabilizer, either a rigid (TAC) or a flexible (FlexTAC) tab is used to augment the functionality of the control surface. The TAC airfoil has three elements while the FlexTAC airfoil has only two. This paper first summarizes CFD validations on the TAC and FlexTAC airfoils using the unstructured U2NCLE and CRUNCH RANS codes for comparisons with water-tunnel data. From the prediction results and the comparisons between the two experimental datasets and the calculations, it is concluded that:

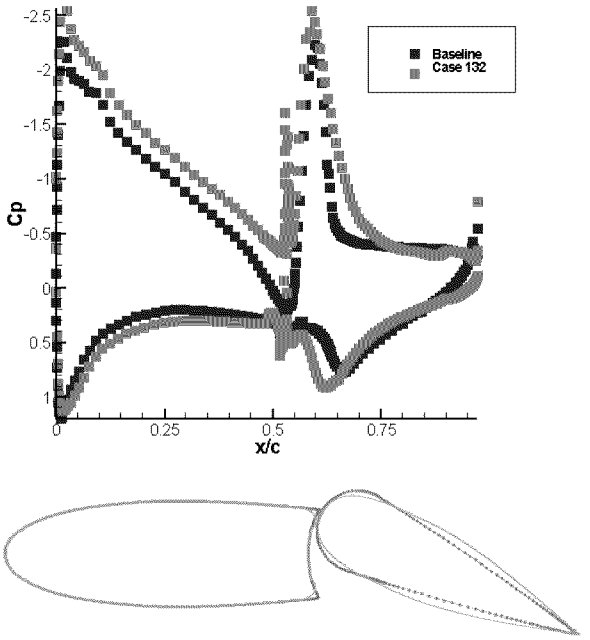

Figure 13: Comparison of the Cp distribution and shape profile of the C132 (blue) and baseline (red) designs

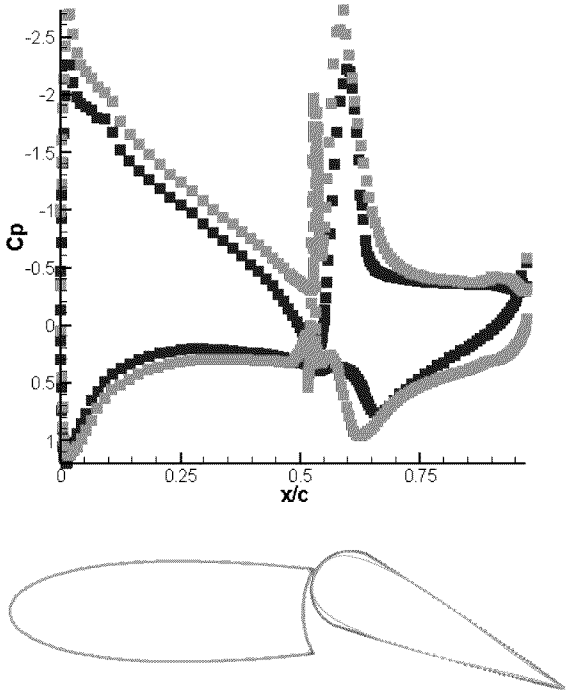

Figure 14: Comparison of the Cp distribution and shape profile of the C46 (blue) and baseline (red) designs

(1) Both the U2NCLE and CRUNCH codes are able to predict the forces and moments with reasonable accuracy for flap angles smaller

than 20 deg. Although both predictions deviate from the measured data for flap angles greater than 20 deg., CRUNCH predicts forces more accurately while U2NCLE predicts better moments.

(2) The comparisons between predictions and measurements indicate that the overall FlexTAC measured forces may have been over-corrected for water tunnel blockage.

(3) The comparisons between the measured and predicted TAC and FlexTAC data suggest that the gudgeons have a profound effect on the stabilizer and flap torque calculations, but have a minimum effect on the force calculations.

(4) Both CRUNCH and U2NCLE predict the trends of the force and moment even at large flap angles. This validation implies they are able to be adapted for optimization calculations. The CRUNCH code was used for the optimization calculations through its scripting capability with the grid generator.

A comprehensive framework for carrying out design optimization studies of complex systems has been developed following the CFD validation. The framework consists of a genetic algorithm coupled with a hybrid unstructured RANS solver and the mesh generator GRIDGEN. The evolutionary algorithm employed in the framework permits global search of the design landscape in a robust manner and permits a complex array of variables and constraints to be specified. Incorporation of a RANS based solver allows the design procedure to take complex flow features such as secondary flows, turbulence etc. into account. The hybrid unstructured RANS procedure allows economy in overall mesh sizes, while permitting increased resolution in regions sensitive to design changes. Furthermore, the hybrid unstructured RANS procedure is very robust and provides fitness evaluations with rapid turnaround time, a key requirement to an efficient design procedure.

The coupled hybrid unstructured RANS framework with the genetic algorithm based design optimization procedure was used for improving the performance of multi-element control surface used in marine vehicles. The RANS framework was necessary for this problem because of strong viscous/turbulent effects in the gap region between the stabilizer and flap that comprise the multi-element control surface. The study is concluded with:

The problem definition includes both modifications to the stabilizer and flap simultaneously, because of the close coupling of the two elements.

Design/optimization studies enhance performance of the multi-element airfoil by identifying designs that reduce operational torque by over three orders of magnitude at the highest angle of attack (25 degrees).

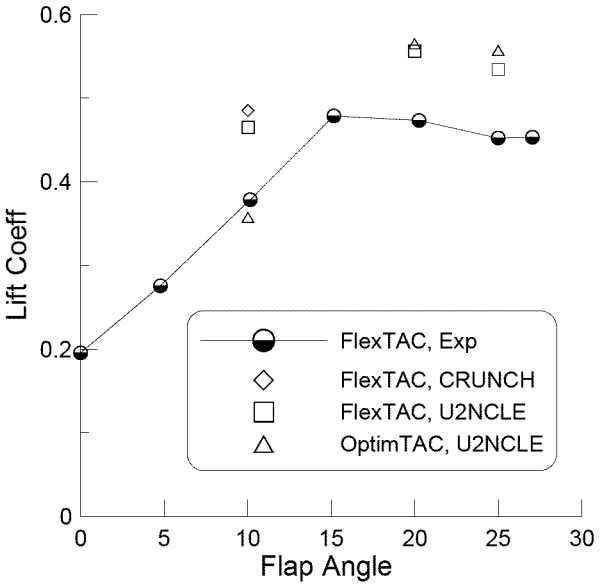

(a)

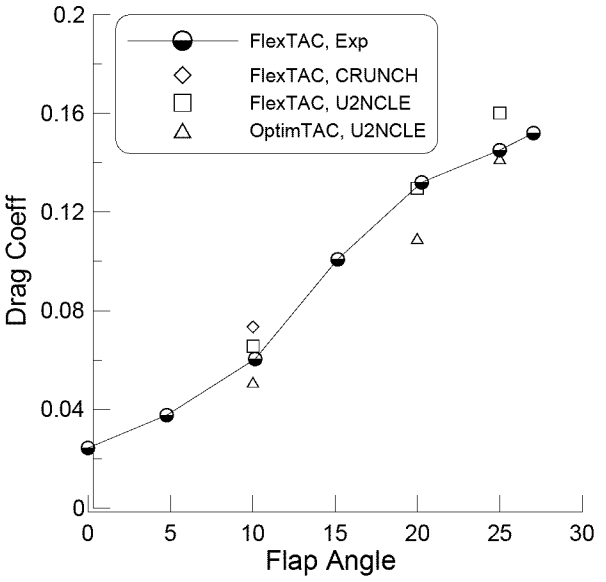

(b)

Figure 15: Comparison of forces between FlexTAC and OptimTAC foils (a) lift; (b) drag

(1) A database of relevant designs is maintained during the optimization process and shapes comprising the database are searched to extract a design that was eventually selected for further RANS and experimental validations.

(2) These designs also show enhanced lift over most of the operational range. The

performance enhancement is mostly achieved by modification of the flow in the gap region between the stabilizer and the flap.

(3) Changes to stabilizer shape ensure smooth flow transition between the stabilizer and the flap.

(4) Shifted peak pressure location on the flap results in a large reduction of the flap torque. Changes to the trailing edge further attribute to the redistribution in pressure, thereby leading to an additional lift along with the reduction in torque.

(5) Comparisons with the 3-D RANS calculations and experimental data further confirm the benefit of the current optimal shape.

ACKNOWLEDGMENTS

Computer resources for the computations described in this paper were provided by the DoD High Performance Computing Modernization Program. Additional computer resources were provided by the United States Navy's SEATECH Center located at NSWCCD. The work was funded by the Naval Sea Systems Command, SUB-RT, as part of the FlexTAC Project.

NOMENCLATURE

C132, C46	foils named during optimization calculations
c_m	mean chord
C_p	pressure coefficient
q	$(k)^{1/2}$
FlexTAC	Flexible TAC
k	turbulent kinetic energy
OptimTAC	3-D foil with C132 cross section
TAC	Tab Assisted Control
TCL/TK	scripting language
V_∞	freestream velocity
α	inflow angle to multi-element foil
ε	rate of dissipation of turbulent kinetic energy
δ_F	flap angle
δ_T	tab angle
ρ	fluid density
ω	ε/k

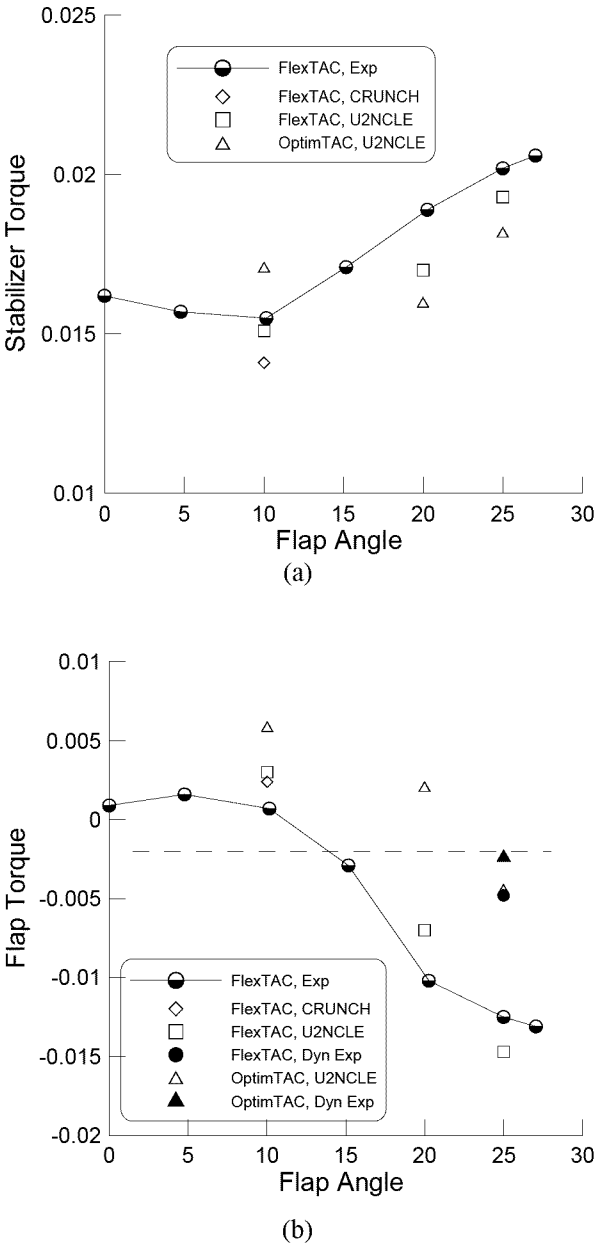

Figure 16: Comparison of moments between FlexTAC and OptimTAC foils (a) stabilizer torque; (b) flap torque

REFERENCES

Ahuja, V., Hosangadi, A. and Arunajatesan, S., "Simulations of Cavitating Flows Using Hybrid Unstructured Meshes," J. of Fluids Engineering, Vol. 123, No. 2, pp. 331-340, 2001.

Cao, H. V. and Blom, G. A., "Navier-Stokes/Genetic Optimization of Multi-Element Airfoils," AIAA paper 96-2487, 1996.

Carpenter, B. and Nguyen, T., "Shape Memory Alloy Actuator for Tab Assisted Control Surface Application", SPIE, Newport Beach, CA, 1999.

Cavallo, P. A., Hosangadi, A., Lee, R. A. and Dash, S. M., "Dynamics Unstructured Grid Methodology with Application to Aero/Propulsive Flowfields," AIAA paper 97-2310, 1997.

Coakley, T. J. and Hsieh, T., "A Comparison between Implicit and Hybrid Methods for the Calculation of Steady and Unsteady Inlet Flows," AIAA Paper 85-1125, 1985.

Gaither, J., Marcum, D. and Mitchell, B., "SolidMesh: A Solid Modeling Approach to Unstructured Grid Generation," the 7th Intern. Conf. on Numerical Grid Generation in Computational Field Simulations, 2000.

Gowing, S., Lee, Y. T., Carpenter, B., Atsavapranee, P. and Hess, D., "FlexTAC: An Advanced Submarine Control Surface and Actuation System," AIAA paper 2004-902, 2004.

Holland, J.H., Adaptation in Natural and Artificial Systems, MIT Press, 1975.

Hosangadi, A., Lee, R. A., York, B. J., Sinha, N., and Dash, S. M., "Upwind Unstructured Scheme for Three-Dimensional Combusting Flows," J. of Propulsion and Power, Vol. 12, No. 3, 1996, pp. 494-503.

Hyams, D. G., Sreenivas, K., Sheng, C., Nichols, S., Taylor, L. K., Briley, W. R., Marcum, D. L., and Whitfield, D. L., "An Unstructured Multielement Solution Algorithm for Complex Geometry Hydrodynamic Simulations," the 24th Sym. On Naval Hydrodynamics, Fukuoka, Japan, July 8-13, 2002.

Lee, Y. T., Ebert, M. P. and Hosangadi, A., "Flow Predictions for Multi-Element Control Surface," NSWCCD-50-TR-2002/061, 2002.

Lee, Y. T., Ahuja, V., Ebert, M., and Hosangadi, A., "Flow Predictions and Shape Optimization of A Multi-Element Airfoil," the 8th Intern. Conf. on Numerical Ship Hydrodynamics, Busan, Korea, July 22-25, 2003.

Marcum, D. and Weatherill, N., "Unstructured Grid Generation Using Iterative Point Insertion and Local Reconnection," AIAA J., Vol. 33, No. 9, 1995, pp. 1619-1625.

Nguyen, T. D., Gowing, S., and Bochinski, D., "Tab-Assisted Control Surface for Marine Application," The Intern. Sym. Warship '99 Naval Submarines, 1999.

So, R. M. C., Sarkar, A., Gerodimos, G., and Zhang, J., "A Dissipation Rate Equation for Low Reynolds Number and Near-Wall Technique," Theor. Comput. Fluid Dyn., Vol. 9, 1997, pp. 47-63.

Sung, C. H., and Rhee, B., "Prediction of Forces and Moments of Rudders with Flap and Tab, Part I. 2D Airfoil with Flap and Tab," the 7th Intern. Conf. on Numerical Ship Hydrodynamics, Nantes, France, July 19-22, 1999.

Sung, C. H., Rhee, B., and Koh, I.-Y., "Validation of Tab Assisted Control Surface Computation," the 23rd Sym. On Naval Hydrodynamics, Bassin D'essair Des Carenes, Val De Reuil, France, Sept. 17-22, 2000.